Fuel 97 (2012) 630–637

Contents lists available at SciVerse ScienceDirect

Fuel

journal homepage: www.elsevier.com/locate/fuel

Partial oxidation of methane on NiO–MgO–ZrO_2 catalysts

Yvan J.O. Asencios [a], Pedro A.P. Nascente [b], Elisabete M. Assaf [a,*]

[a] Instituto de Química de São Carlos, Universidade de São Paulo, 13560-970 São Carlos-SP, Brazil
[b] Departamento de Engenharia de Materiais, Universidade Federal de São Carlos, 13565-905 São Carlos-SP, Brazil

ARTICLE INFO

Article history:
Received 27 October 2011
Received in revised form 27 February 2012
Accepted 29 February 2012
Available online 13 March 2012

Keywords:
Catalyst
Polymerization-method
Solid solutions
POM
Synthesis gas

ABSTRACT

Catalysts containing mixtures of NiO, MgO and ZrO_2 were synthesized by the polymerization method. They were characterized by X-ray diffraction (XRD), physisorption of N_2 (BET), X-ray photoelectron spectroscopy (XPS) and X-ray absorption near-edge structure (XANES), and then tested in the partial oxidation of methane (POM) in the presence of air ($2CH_4$:$1O_2$) at 750 °C for 6 h. Among the ternary oxides, the catalyst with 40 mol% MgO showed the highest conversion rates in the catalytic processes, but also the highest carbon deposition values (48 mmol h^{-1}). The greater the amount of NiO–MgO solid solution formed, the higher was the conversion rate of reactants (CH_4), peaking at 40 mol% of MgO. Catalysts with lower Ni content on the surface achieved a high rate of CH_4 conversion into synthesis gas (H_2 + CO). The formation of more NiO–MgO solid solution seemed to inhibit the deactivation of Ni° during reaction. The values of the H_2/CO product ratio were generally found to be slightly lower than stoichiometric.

1. Introduction

In recent years, the conversion of methane to synthesis gas (syngas) has become one of the most important topics in catalysis research. Syngas (a mixture of CO and H_2) can be used to synthesize methanol, which is employed in the energy sector (e.g. methanol fuel cells). Syngas can also be used in the Fischer–Tropsch process to produce diesel and synthetic gasoline [1–4]. Synthesis gas is commonly obtained by steam reforming of methane (SRM) at 800 °C [5]:

$$\text{SRM}: \quad CH_4 + H_2O \rightarrow CO + 3H_2 \quad \Delta H^\circ = 225.4 \text{ kJ mol}^{-1} \tag{1}$$

However, this process provides H_2/CO ratios too high for the Fischer–Tropsch process and methanol synthesis. In recent years, much research has been done on the conversion of methane into synthesis gas by dry reforming of methane (DRM [5]) and by partial oxidation of methane (POM [6]):

$$\text{DRM}: \quad CH_4 + CO_2 \rightarrow 2CO + 2H_2 \quad \Delta H^\circ = 260.5 \text{ kJ mol}^{-1} \tag{2}$$

$$\text{POM}: \quad CH_4 + 1/2O_2 \rightarrow CO + 2H_2 \quad \Delta H^\circ = -22.6 \text{ kJ mol}^{-1} \tag{3}$$

According to reaction (2), POM is a mildly exothermic reaction and, as a result, rather hard to control, especially in a large-scale reactor. On the other hand, this reaction has some advantages, two of which are the desirable H_2/CO ratio of 2, favorable both to methanol synthesis and the Fischer–Tropsch process, and the high selectivity [6].

The available literature [7–12] mentions three main types of catalysts for POM: (i) the non-noble group VIII metals, nickel, cobalt and iron, (ii) the noble group VIII metals (Ru, Rh, Pd, Pt, Ir) and (iii) transition metal carbide catalysts. Noble metal-based catalysts have proved effective in the POM and highly resistant to coke formation [13], but their rareness and high cost limit their use. Among the non-noble metals, Ni-based catalysts have shown similar activity to those based on noble metals and have attracted much attention, due to their low cost. However, they suffer rapid deactivation due to coking (carbon deposition), during DRM or POM catalysis.

Among several hypotheses on the mechanism of coke formation on nickel catalysts, two reactions stand out as being probably the most important: methane cracking (reaction (4)) and the Boudouard reaction (reaction (5)):

$$CH_4 \rightarrow C + 2H_2 \quad \Delta H^\circ = 74.8 \text{ kJ mol}^{-1} \tag{4}$$

$$2CO \rightarrow C + CO_2 \quad \Delta H^\circ = -172.8 \text{ kJ mol}^{-1} \tag{5}$$

In POM reactions with Ni catalysts, it is thought that coke is formed mainly by the methane cracking reaction [14,15]. During the POM, oxygen species adsorbed on the surface of the catalyst may remove the coke deposited on the surface by forming CO. However, on several catalysts, especially non-noble metals such Ni, not all the coke is removed, perhaps due to insufficient activated O_2 molecules and/or the high relative solubility of carbon

* Corresponding author.
E-mail address: eassaf@iqsc.usp.br (E.M. Assaf).

0016-2361/$ - see front matter © 2012 Elsevier Ltd. All rights reserved.
http://dx.doi.org/10.1016/j.fuel.2012.02.067

in nickel. In this context, research focused on improving the activation of reactant molecules such as O_2 and thus suppressing the build-up of carbon on the catalytic surface becomes very relevant. Some studies indicate that the use of mixed oxides such as CeO_2/ZrO_2 [16], Y_2O_3/ZrO_2 [8], TiO_2/ZrO_2 [13] and Nb_2O_5/ZrO_2 [17] as carriers can enhance the performance of the catalyst in the POM, relative to the pure oxides.

Solid solution of NiO/MgO is a good catalyst for the SRM, POM and DRM reactions, because this solid solution promotes fine dispersion of the nickel metal on reduction of the oxide and inhibits the formation of large clusters of Ni° that result in Ni° sintering at high temperatures, thus inhibiting carbon deposition. However, this catalyst has poor mechanical strength (which is important in industrial applications) and its activity is strongly impaired when it is added to typical supports, such as SiO_2 or Al_2O_3 [6]. Al_2O_3 is a common catalytic support, with high thermal stability, but its acidity leads to deactivation of nickel catalysts by coke deposition [10].

Pompeo et al. [4] demonstrated that, in DRM and POM, $Ni/\alpha–Al_2O_3$ catalysts improve their activity and stability when ZrO_2 is added to the catalytic support. This additive seems to inhibit carbon formation during the reaction. According to those authors, ZrO_2 promotes the gasification of CO_x intermediates and thus promotes removal of deposited carbon. Moreover, the properties of ZrO_2, in particular its oxygen conductivity and thermal stability, can be modified by adding lanthanide or alkaline earth oxides [18].

Another study, by Dong et al. [19], on SRM, DRM and POM on $Ni/Ce–ZrO_2$ catalysts, showed that these catalysts have high activity and stability because of the presence of two types of active center: one actives the molecule of CH_4 and the other, the O_2 or H_2O molecules. Those authors concluded that the oxygen conductivity of $CeO_2–ZrO_2$ is beneficial to SRM, DRM and POM reactions.

In a previous report [20], we demonstrated that the addition of small amounts of MgO to the Ni/ZrO_2 catalyst improved its performance in the catalysis of biogas reforming, because of the formation of oxygen vacancies ($MgO–ZrO_2$) and a NiO–MgO solid solution. The aim of the present study was to explore further the role of the NiO–MgO solid solution in the POM reaction carried out on $NiO–MgO–ZrO_2$ catalysts. To this end, Ni catalysts with a wider range of contents of MgO were synthesized and studied under reaction conditions.

2. Experimental

2.1. Preparation of catalysts

The catalysts were prepared by the one-step polymerization method, which has been given in detail in the previous paper [20]. Three salt precursors were mixed together: $Ni(NO_3)_2{\cdot}6H_2O$ (Aldrich); $Zr(CO_3)_2{\cdot}1.5H_2O$ (Aldrich) and $Mg(NO_3)_2{\cdot}6H_2O$ (Mallinckrodt), all of 99.9% purity. The MgO content was varied from 4 to 40 mol% (relative to ZrO_2). The nickel content remained constant at 20 wt%. The products were heated at 10 °C min^{-1} to 500 °C and calcined at this temperature for 3 h and then at 750 °C for 2 h, in synthetic air. Catalysts were designated as Ni4MZ, Ni20MZ and Ni40MZ, according to the molar percentage of MgO in the catalysts. Additionally, two samples were synthesized under the same conditions as the catalysts, one containing only NiO–MgO solid solution (sample NiM) and the other without this solid solution (NiO plus ZrO_2, sample NiZ).

2.2. Characterization

The crystal phases were identified with a Rigaku Multiflex X-ray diffractometer (40 kV, 30 mA) scanning in the range 2θ = 5–80° at 2° min^{-1}, using Cu Kα radiation (λ = 1.5406 Å). The specific surface area was estimated by the BET method from N_2 adsorption/desorption isotherms at liquid nitrogen temperature, using a Quantachrome Nova 1200 instrument. The composition of the catalysts was determined by energy-dispersive X-ray spectroscopy (EDX), using a LEO 440 scanning electron microscope with a tungsten filament coupled to an energy-dispersive X-ray detector. The samples were made up in the form of pellets and coated with a layer of gold to avoid a build-up of charge. X-ray photoelectron spectroscopy (XPS) analyses were performed, employing a surface spectrum microscope (Kratos XSAM HS). The catalysts were analyzed in an ultra-high vacuum environment, using MgKα (1253.6 eV) radiation to excite photoelectrons, generated at a voltage of 11 kV and an emission of 4 mA, resulting in a power of 44 W. The value 284.8 eV, for C 1s of C—C and/or CH, was used as a reference for binding energy.

In situ H_2-TPR/X-ray absorption near edge structure (XANES) studies were performed by dispersive-geometry X-ray absorption spectroscopy at the D06A-DXAS beamline of the Brazilian Synchrotron Light Laboratory (LNLS) in Campinas, Brazil. A Si(1 1 1) monochromator was used to select the energy, and the beam was focused at the sample. The experimental setup has been described in more detail by Meneses et al. [21]. The catalyst sample (pellet) was fixed in a stainless steel holder placed in the center of the quartz tube, and oriented relatively to the beam by fine adjustment of the position of the table. The reactor was purged with He flowing at 30 mL min^{-1} for 15 min, and the reducing gas ($5\%H_2/N_2$) then flowed through the samples (30 mL min^{-1}), while a temperature ramp of 10 °C min^{-1}, from room temperature to 800 °C, was applied by the furnace and XANES spectra were collected at each temperature step. Following this, the XANES spectra were acquired in situ under reaction conditions, the previously reduced catalyst being analyzed under CH_4 (15.4 mL/min, $20\%CH_4$/He) and O_2 (10.4 mL, $5\%O_2$/He) streams for 30 min at 750 °C.

The Ni K-edge spectra were recorded in transmission mode and collected in a CCD detector with 15 ms exposure time and 50 scans for each spectrum. A Ni foil spectrum was recorded to calibrate the photon energy. All spectra were collected in the range from 8200 to 8550 eV.

2.3. Catalytic tests

Catalytic reactions were carried out in a fixed- bed down-flow quartz reactor (i.d. = 10 mm) connected in-line to a gas chromatograph. Prior to reactions, the catalysts were activated by reduction with H_2 (30 mL min^{-1}) at 800 °C for 1 h. The reactions were carried out at 750 °C with a mixture of inlet gases in molar proportion $2CH_4{:}1O_2$, stoichiometric for POM, flowing at 107.5 mL min^{-1}, and 100 mg of catalyst. The oxygen was added in the form of synthetic air ($79\%N_2$, $21\%O_2$). The reaction temperature was measured and controlled by a thermocouple inserted directly into the top of the catalyst bed.

Unconverted reactants and the reaction products were analyzed in-line by a gas chromatograph (Varian, Model 3800) equipped with two thermal conductivity detectors (TCDs) and an automated injection valve. The products at the reactor outlet were divided into two streams which were analyzed differently, to obtain an accurate and complete analysis of the reaction products. In one of the streams, hydrogen and methane were separated on a 13X molecular sieve packed column, with nitrogen as carrier gas. In the other, N_2, CO_2, CH_4 and CO were separated on a Porapak-N packed column, with helium as carrier. Separated gases were monitored at each outlet with a TCD.

Carbon deposition was determined as the apparent gain in mass of the catalyst during the reaction.

The CH_4 conversion was calculated as:

$$X_R(\%) = (\text{Mols } R \text{ in} - \text{Mols } R \text{ out})/(\text{Mols } R \text{ in})$$

The H_2, CO, CO_2 selectivity was calculated as:

$$\text{Mol } i \text{ prod.}/\text{Mol}CH_4 \text{ conv} = \text{Mols of } i \text{ produced}/\text{Mols of } CH_4 \text{ converted}$$

where $R = CH_4$ and i = product (H_2, CO_2 or CO).

3. Results and discussion

3.1. Catalyst characterization

The surface areas of the catalysts are shown in Table 1. As was previously reported [20,18], the monotonic growth of the surface area with MgO content above 4% can be explained by the segregation of MgO particles on the surface. Table 1 also shows the chemical composition of the catalysts. The measured content of Ni (atomic%) was very similar to the theoretical value for each component of the catalysts.

The XRD patterns of samples were shown in a previous report [20], where it was demonstrated that the monoclinic phase of ZrO_2, only observed in the samples NiZ and Ni4MZ, disappeared with larger amounts of MgO (in samples Ni20MZ and Ni40MZ), while the peaks ascribed to the tetragonal phase of ZrO_2 (JCPDS 17-923) were present in all samples. The tetragonal ZrO_2 structure was favored by the dissolution of MgO in ZrO_2, which affected the lattice parameter, calculated from the (1 1 1) peak for tetragonal ZrO_2 (Table 1). According to these values (all of which are lower than that for pure ZrO_2 (5.10 Å)), the ZrO_2 crystal lattice suffered a contraction, probably caused by Mg^{2+} ions substituting some Zr^{4+} ions in the ZrO_2 lattice, since the ionic radius of Mg^{2+}(0.57 Å) is smaller than that of Zr^{4+} (0.59 Å) [22]. The contraction increased as more MgO was added. In the nomenclature of Kroger and Vink [23], the formation of oxygen vacancies in the MgO–ZrO_2 solid solution can be represented by the following equation:

$$MgO + Zr_{Zr}^{x} + O_{o}^{x} \leftrightarrow Mg_{Zr}'' + V_o\square + ZrO_2 \quad (6)$$

where Zr_{Zr}^{x} and O_{o}^{x} are zirconium cation and an oxygen anion in regular positions in the crystal lattice, Mg_{Zr}'' a magnesium cation at the zirconium site and $V_o\square$ a negatively-charged oxygen vacancy in place of the anion O_{o}^{x}.

The formation of the NiO–MgO solid solution led to an enlargement of the lattice parameter of NiO (Table 1). This is readily explained by the fact that the ionic radius of Mg^{2+}(0.57 Å) is larger than that of Ni^{2+}(0.55 Å [22,24,25]) and confirms that Mg^{2+} cations entered the cubic lattice of NiO. The parameter increases on further addition of MgO. In the notation of Kroger and Vink [23], the substitutional solid solution of MgO in NiO can be represented by the following equation:

$$MgO + Ni_{Ni}^{x} \leftrightarrow Mg_{Ni}^{x} + O_{o}^{x} \quad (7)$$

where Ni_{Ni}^{x} is a nickel cation in a regular position in the NiO crystal lattice, Mg_{Ni}^{x} a magnesium cation in place of nickel in the crystal lattice and O_{o}^{x} an oxygen anion in a regular position in the crystal lattice.

The reducing profile of the nickel catalysts was investigated by TPR-XANES analysis. The pre-edge peak intensity and white line intensity were considered the main characteristics for monitoring the reduction of the NiO species. The Ni K-edge XANES spectra for samples NiZ, Ni4MZ, Ni20MZ, Ni40MZ and NiM, analyzed in situ during the reduction reaction ($NiO + H_2 \rightarrow Ni^{\circ} + H_2O$), are shown in Fig. 1a–e. For all catalysts, the first spectrum at room temperature resembles that of NiO (Fig. 1f), with a high intensity white line caused by the Ni–O interaction [26].

A pre-edge feature is also observed, which is due to the forbidden dipole and allowed quadrupole transitions from the Ni 1s orbital to the Ni 3d orbital [27]. As the temperature is increased under reduction with H_2, the intensity of the white line falls and the spectrum assumes a profile like that of Ni°, showing that NiO is reduced to Ni°.

Fig. 1a shows that the reduction of the NiZ catalyst occurred in two steps, the first starting from 300 °C, where a slight decrease in the intensity of the white line was observed. The second step began at 420 °C, where the intensity fell sharply until the spectrum was like that of Ni°. It may be concluded that there were NiO species interacting differently with the support in NiZ, probably NiO interacting weakly (reduced at low temperature) and strongly (reduced at high temperature) with the surface of the support. The same effect was observed in Ni4MZ (with the two different regions at 420 °C and 520 °C) and Ni20MZ (regions at 450 °C and 620 °C). The Ni40MZ sample showed a single reducing region that began at 470 °C, implying that, due to the high MgO content, NiO species were formed on the support in a very homogeneous environment. The NiM sample did not show a perceptible reducing profile, because of the formation of NiO–MgO solid solution. Furthermore, as the MgO content in the mixture was increased, the reducing temperature shifted continuously to higher values, indicating that the strong ionic interaction between MgO and NiO probably hindered the reduction of NiO, owing to the formation of a NiO–MgO solid solution [25]. The relatively low reducing temperature of NiZ is expected, since it is known that NiO interacts only weakly with ZrO_2 [20].

Photoelectron spectroscopy was used to obtain further information about the valence/oxidation state of the elements and the surface composition of the NiO–MgO–ZrO_2 catalysts. The change in coordination number of Zr atoms (between monoclinic and tetragonal crystal lattices) is confirmed by the change in the measured binding energies (BE) of Zr $3d_{5/2}$ core levels (Table 2). The BE for Zr in NiZ of 182 eV is very close to the theoretical value for the Zr in ZrO_2 (182.1 eV) [28]. This value decreased in samples Ni4MZ, Ni20MZ and Ni40MZ. This decrease can be interpreted in terms of electron transfer from Mg^{2+} to Zr^{4+}, because as the MgO content increased, BE values for Mg increased (from 48.5 eV in Ni4MZ to 49.7 eV in Ni40MZ). This is consistent with the XRD analysis, where it was shown that MgO and ZrO_2 form a solid solution.

According to the literature [29,30] the theoretical value of BE for Ni $2p_{3/2}$ in Ni^{2+} (in stoichiometric NiO) is 855 eV. This value is very close to that of Ni^{2+} in NiZ, showing that the addition of ZrO_2 did not affect the environment of Ni, probably due to the weakness

Table 1
Physicochemical properties and chemical composition of catalysts analyzed by EDX (theoretical values are in brackets).

Catalysts	Lattice parameter (Å) a (ZrO_2) a (NiO)	Surface area ($m^2\ g^{-1}$)	Chemical analysis (%)			
			Mg (at%)	Ni (at%)	Zr (at%)	
NiZ	5.090	4.15	16	–	39.7(34)	60.3(66)
Ni4MZ	5.083	4.16	16	1.2(2)	34.4(34)	64.4(64)
Ni20MZ	5.074	4.17	23	5.4(11)	34.8(32)	59.8(57)
Ni40MZ	5.052	4.18	26	10.0(20)	31.4(30)	58.6(50)
NiM	–	4.18	34	85.6(85)	14.4(15)	–

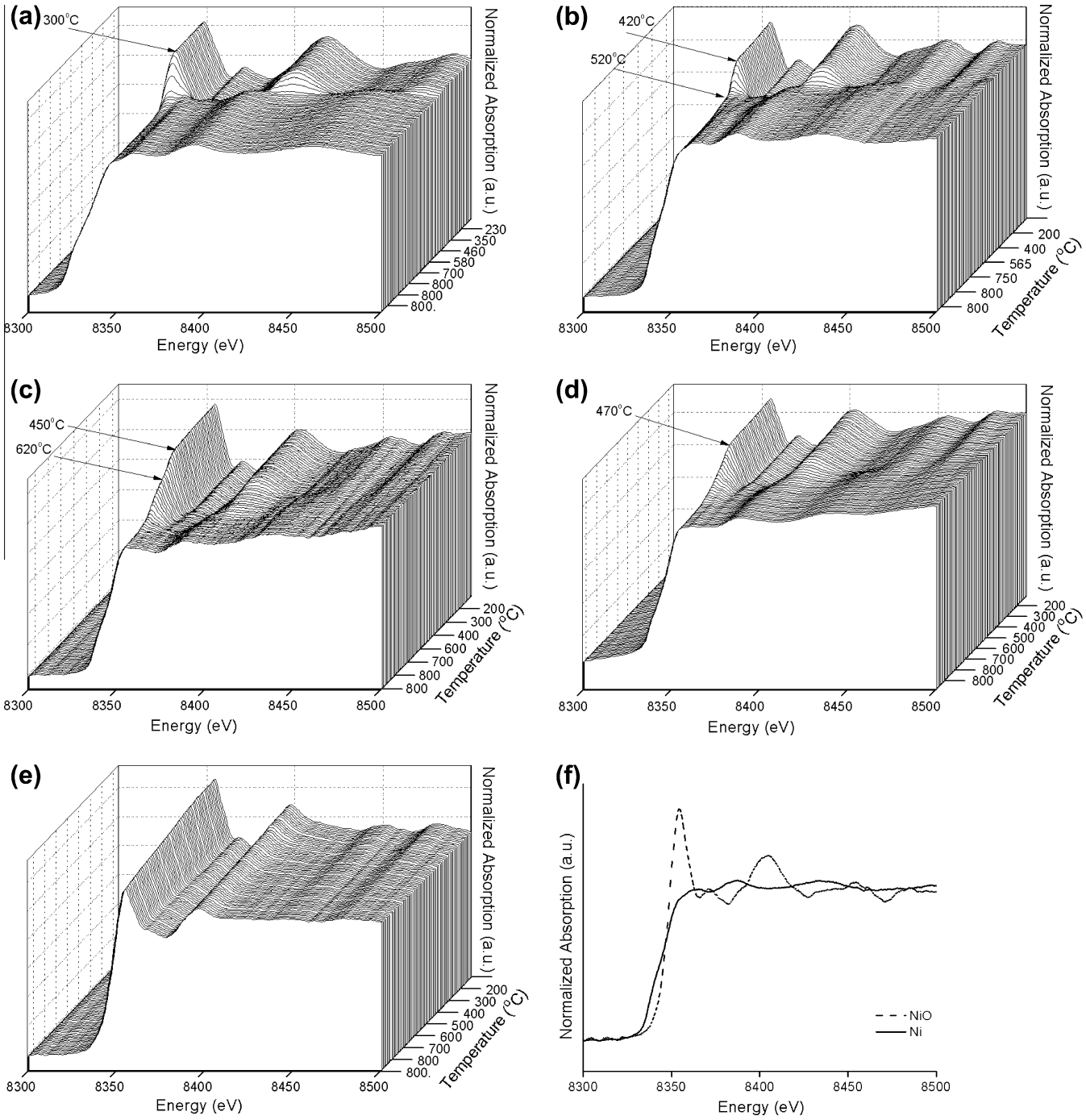

Fig. 1. TPR-XANES of catalyst: (a)NiZ, (b)Ni4MZ, (c)Ni20MZ, (d)Ni40MZ and (e)NiM; and (f) Ni K-edge XANES spectra of NiO and Ni foil.

Table 2
Binding energies (eV) of principal peaks for calcined catalysts.

Catalysts	Binding energies (eV)		
	Zr $3d_{5/2}$	Ni $2p_{3/2}$	Mg 2p
NiZ	182.0	855.1	–
Ni4MZ	181.7	854.6	48.5
Ni20MZ	181.9	855.0	49.6
Ni40MZ	181.9	854.8	49.7
NiM	–	855.3	49.6

of the interactions between NiO and ZrO_2. In the NiM sample, the BE for Ni (855.3 eV) was higher than the value of Ni in NiO (855 eV), while the BE for Mg (49.6 eV) was lower than that of Mg in MgO (50.5 eV), showing that electron transfer from NiO to MgO took place. This strengthened the interaction between these oxides, which formed a solid solution [5]. The non-uniform variation of the BE for Ni in Ni4MZ, Ni20MZ and Ni40MZ, may be explained in terms of various interactions among the NiO and ZrO, and NiO and MgO species, probably favored by the mixing of the three oxides together in the one-step polymerization method.

The degrees of dispersion of nickel, magnesium and zirconium atoms on the surface of the catalysts, estimated by XPS, are shown in Table 2. From these values, as expected, the surface of NiO–MgO–ZrO_2 catalysts was enriched in MgO as the Mg load increased (Ni20MZ, Ni40MZ and NiM samples); conversely, zirconium atoms

decreased as the Mg load increased. Simultaneously, the quantity of Ni on the surface fell. This effect may be due to the strong interaction between NiO and MgO in the solid solution, which probably favors the transport of nickel atoms into the bulk.

Finally, there is a large amount of nickel on the surface of sample NiZ, compared to that on the surface of the other samples, owing to the weak interaction between NiO and ZrO_2 (as found in TPR-XANES analyses) that did not favor the internal diffusion of NiO into the bulk.

3.2. Catalytic activity

Fig. 2 shows the profiles of CH_4 conversion (a) and the H_2/CO ratios in products (b) against time on stream. The highest conversions were achieved on NiM, Ni40MZ and Ni20MZ. It can be seen that the conversion rate decreased as follows: NiM > Ni40MZ = Ni20MZ > Ni4MZ > NiZ; in other words, with falling MgO content. Catalytic activity was very similar on Ni40MZ and Ni20MZ. The rates of carbon deposition rose monotonically with MgO content: on the catalysts NiZ, Ni4MZ, Ni20MZ, Ni40MZ and NiM they were 7, 8, 12, 48, and 64 mmol h^{-1}, respectively. These values indicate that Ni20MZ showed the most balanced performance in the POM reaction, because it achieved a high rate of conversion (Fig. 2a) and relatively low carbon deposition, as well as the highest value of H_2/CO (Fig. 2b). The highest H_2/CO ratios were produced by samples Ni20MZ, Ni40MZ and NiM: around 1.7, which is nearly stoichiometric. The low values of H_2/CO for NiZ and Ni4MZ are in agreement with the low conversion values seen on these catalysts.

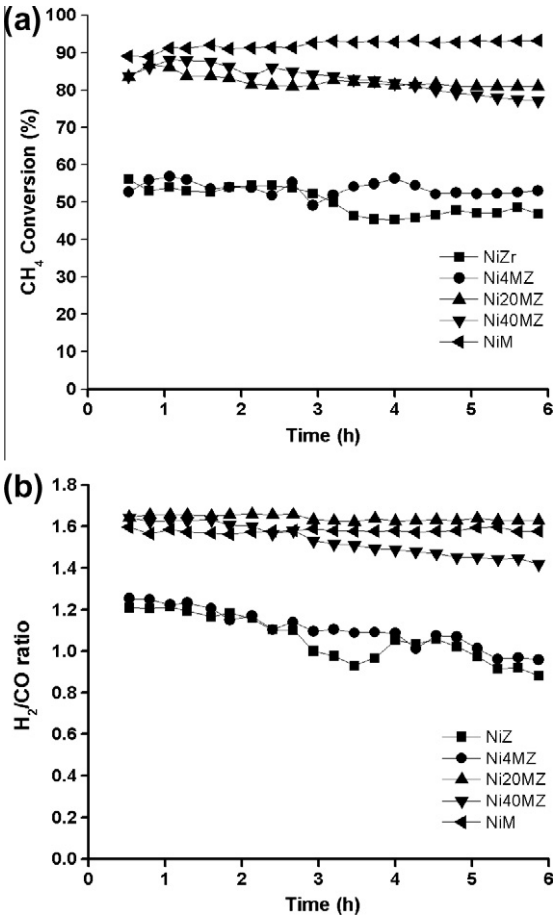

Fig. 2. Partial oxidation of methane on catalysts over 6 h: (a) conversion of CH_4, and (b) H_2/CO ratios in products (conditions: T = 750 °C, CH_4/O_2 = 2/1).

The value and variation of the H_2/CO relative to the stoichiometric value (approximately 2) can be explained in term of reactions occurring in parallel with the POM reaction.

Two general mechanisms have been proposed for the POM reaction to produce synthesis gas: (i) the combustion-reforming mechanism, in which CO_2 and H_2O are the primary products of the total combustion of methane (TCM), which is followed by dry reforming of methane (DRM) and steam reforming of methane (SRM) to produce syngas [10]; (ii) the pyrolysis mechanism, in which the syngas is produced directly [8]. In both cases CO and H_2 are the final products, with the stoichiometric H_2/CO ratio of 2. However, in this

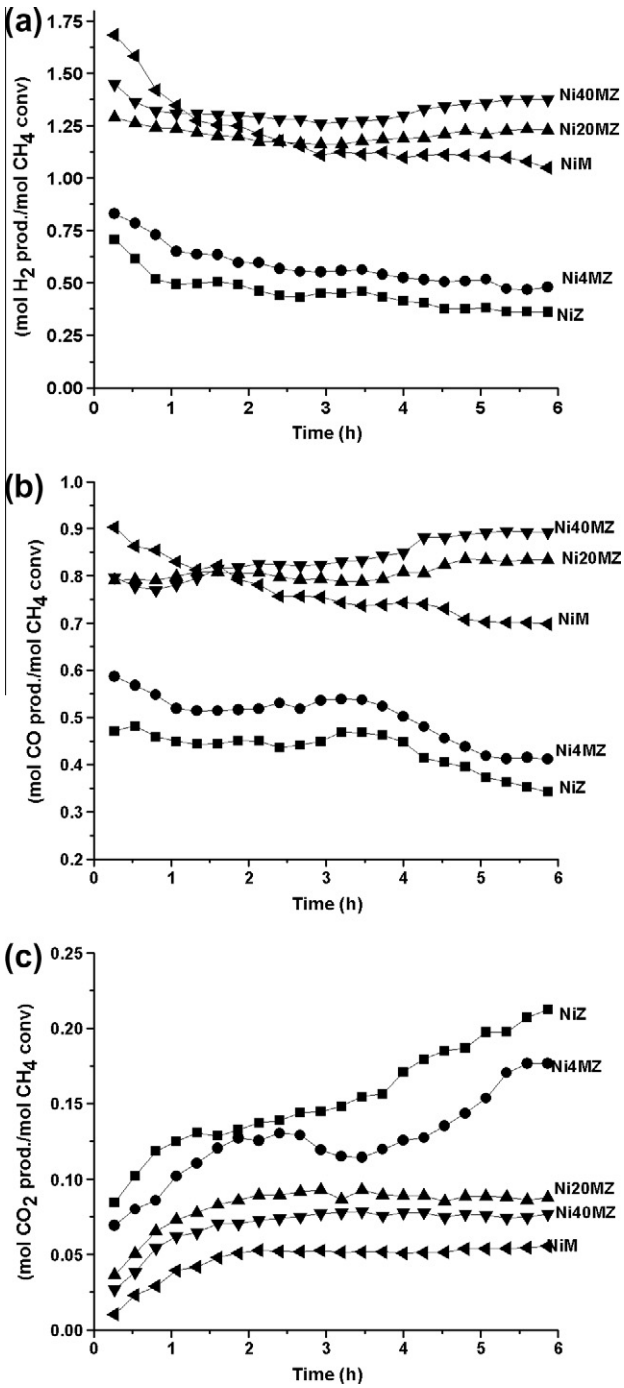

Fig. 3. Selectivity of the catalysts in the partial oxidation of methane over 6 h: (a) selectivity of H_2, (b) selectivity for CO, and (c) selectivity of CO_2 (conditions: T = 750 °C, CH_4/O_2 = 2/1).

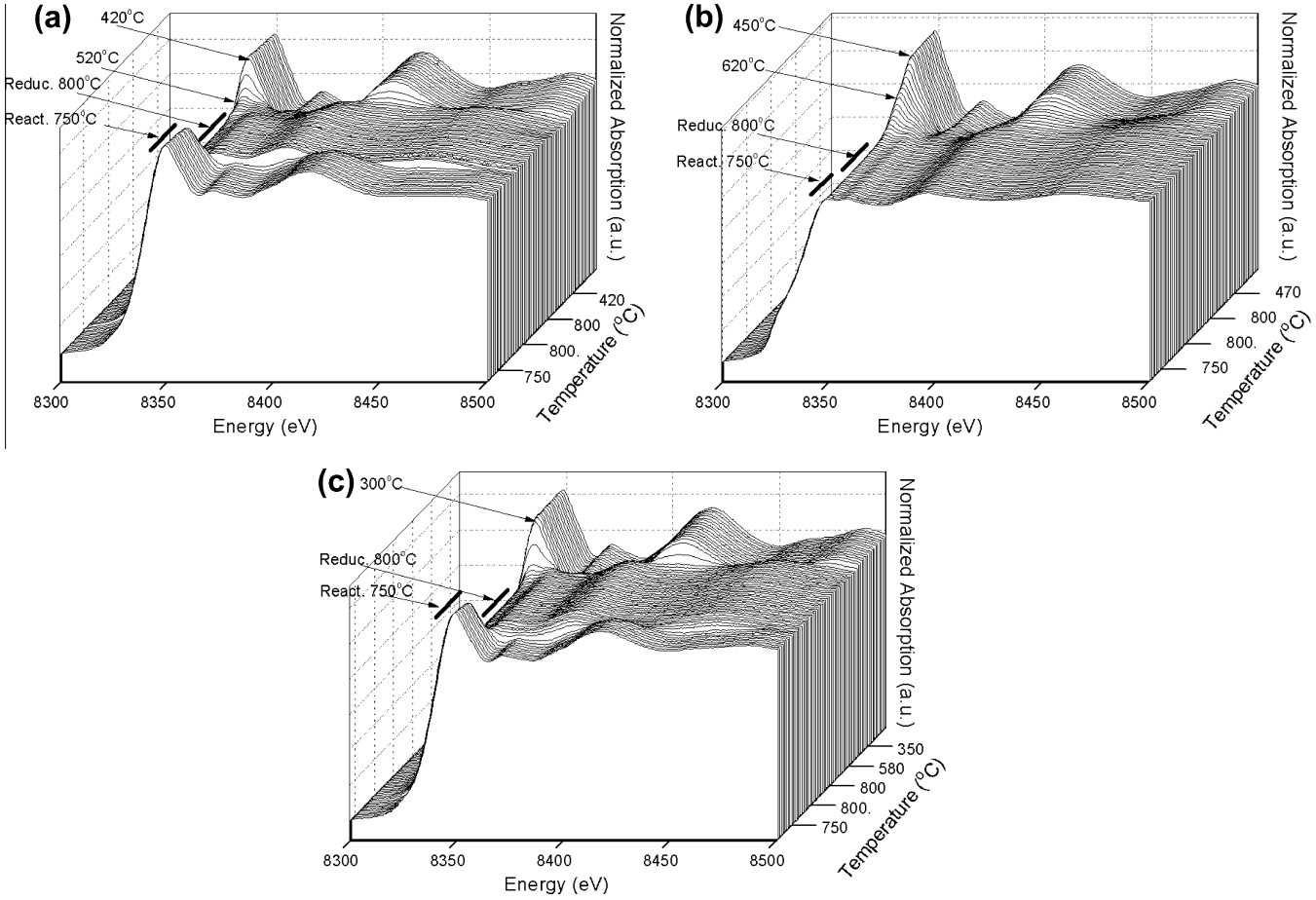

Fig. 4. POM-XANES profiles of catalyst: (a)Ni4MZ, (b)Ni20MZ, and (c)NiZ.

study, traces of H_2O were collected and CO_2 was found during each catalytic test, so that the combustion-reforming mechanism occurred on these catalysts. The combustion-reforming mechanism of the POM reaction is described [10] by the following reactions:

$$\text{TCM}: \ CH_4 + 2O_2 \leftrightarrow CO_2 + 2H_2O \quad \Delta H^\circ = -890 \text{ kJ mol}^{-1} \tag{8}$$

$$\text{DRM}: \ CH_4 + CO_2 \leftrightarrow 2CO + 2H_2 \quad \Delta H^\circ = 260.5 \text{ kJ mol}^{-1} \tag{2}$$

$$\text{SRM}: \ CH_4 + H_2O \leftrightarrow CO + 3H_2 \quad \Delta H^\circ = 225.4 \text{ kJ mol}^{-1} \tag{1}$$

Moreover, as CO_2 was found in the catalytic test, and H_2 was a product of the reaction, the reverse water–gas shift reaction (WGSR) (9) is very likely to occur, as it is known that this reaction is favored at high temperature. This reaction consumes H_2 and CO_2 to produce CO and H_2O:

$$\text{Reverse WGSR}: \ CO_2 + H_2 \leftrightarrow CO + H_2O \quad \Delta H^\circ = 34.3 \text{ kJ mol}^{-1} \tag{9}$$

The occurrence of the WGSR and the occurrence of TCM as the initial and rapid step in POM may explain why the H_2/CO ratio does not reach the stoichiometric value. Given that the molar ratio of reactants CH_4:O_2 in the feed is 2 and that POM proceeds by reactions (8), (2), and (1), then according to the stoichiometry, the value of H_2/CO should be 2, which would indicate that the reactions DRM and SRM occur in parallel. Ericksson et al. [11] found a H_2/CO ratio close to 3, which they attributed to a greater contribution of

Table 3
Atomic ratios for calcined catalysts.

Catalysts	Atomic ratios (%)		
	Mg	Ni	Zr
NiZ	–	25	75
Ni4MZ	9	16	76
Ni20MZ	16	14	70
Ni40MZ	32	12	56
NiM	90	10	–

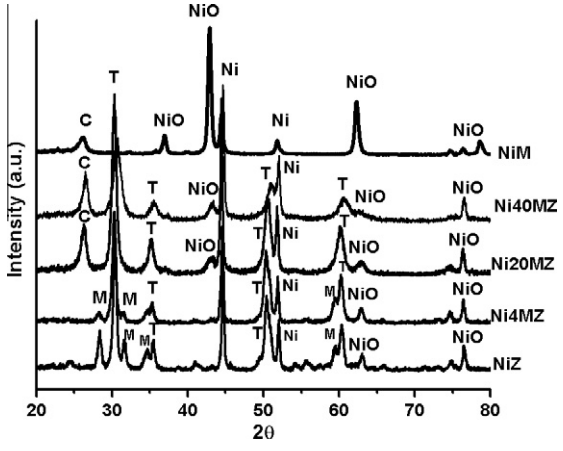

Fig. 5. XRD patterns of catalysts after 6 h of reaction: tetragonal ZrO_2 (T), monoclinic ZrO_2 (M), graphitic carbon (C).

SRM than of DRM to the reaction. The values of H_2/CO ratio found in the present study (Fig. 2b) demonstrate that SRM and DRM make similar contributions.

To explore the catalytic tests, in more detail, selectivity results for H_2, CO and CO_2 are shown in Fig. 3. According to these results, the selectivity for H_2 and CO followed a similar trend to that of CH_4 conversion, in that NiZ and Ni4MZ showed the lowest selectivity for H_2 and CO. Despite the fact that NiM sample had the highest methane conversion rates, its selectivity for H_2 and CO decreased continuously during the reaction. It is probable that this catalyst breaks the C—H bonds readily, to form coke (the highest amount of coke was recorded on this sample), but does not have sufficient active sites for decomposition of O_2 molecules ($O_{2(g)}$ + active site → $2O_{(s)}$ [31]), owing to the absence of MgO–ZrO_2 solid solution.

In generals, samples showed low selectivity for CO_2, NiZ and Ni4MZ being the most selective for CO_2, among all samples. Furthermore, the selectivity to CO and H_2 of samples NiZ and Ni4MZ tended to decrease continuously during the reaction, implying that the reverse WGSR and/or TCM were more favored during the reaction. The trend found in CO_2 selectivity, indicates that the addition of more MgO to the catalysts led to lower production of CO_2; probably due to the formation of more oxygen vacancies, which activate CO_2 molecules (CO_2 + active site → CO + $O_{(s)}$ [31]), as well as the basic character of the MgO added (which forms intermediate carbonate species that decompose rapidly), favoring the conversion of CO_2 in the POM reaction. The role of basic additives (e.g. MgO) in the catalysis of DRM reactions has been studied previously and details are found in the literature [32,33].

From the above analysis, we propose that the NiO–MgO–ZrO_2 catalyst has two types of active site: the first is the Ni° active centre that dissociates CH_4 molecules and the second is the oxygen vacancy that activates the O_2 and CO_2 molecules. Furthermore, it is possible that the NiO–MgO solid solution formed favored an optimal dispersion of Ni°, increasing the number of its active sites and thus increasing the conversion of CH_4. During these reactions, the oxygen vacancies generated by the MgO–ZrO_2 solid solution can speed up the dissociation and transferral of adsorbed oxygen (by activating O_2 molecules) [34,35], assisting in coke removal and thus resulting in higher stability of the POM reaction.

The POM-XANES analyses were carried out to explore further the state of the nickel metal on the catalyst during the POM reaction, for the best (Ni20MZ) and the two worst catalysts (Ni4MZ and NiZ). The results are shown in Fig. 4a–c. They reveal that the low POM activity of samples NiZ and Ni4MZ can be explained by the oxidation of Ni° active centers, because, according to Fig. 4a and c, under reaction conditions (in a stream of CH_4 and O_2 and the reaction products formed: H_2, CO, CO_2 and H_2O) introduced immediately after the TPR reduction processes, the XANES profile returns to that of NiO. Moreover, as discussed above, the samples NiZ and Ni4MZ have a relatively high selectivity for CO_2 (Fig. 3). Thus, we propose that the presence of CO_2 and H_2O, and the O_2 of the inlet stream, favors the oxidation of Ni° particles on the surface of these samples. In other words, the presence of O_2, H_2O and CO_2 in the stream affected adversely the catalytic performance of these two samples.

As seen in the surface atomic ratios shown in Table 3, NiZ and Ni4MZ had more nickel on the surface than Ni20MZ, probably in aggregated form, so that in these samples these Ni° particles may have been in positions that favor their oxidation to NiO. In the sample of Ni20MZ, which had a lower nickel content on the surface and a relatively high MgO content (resulting in greater formation of NiO–MgO solid solution), Ni° particles were finely dispersed and not so readily oxidized to NiO. It appears that a larger amount of NiO–MgO solid solution in samples inhibited deactivation of the catalyst, as the sample with 20% of MgO (Ni20MZ) showed no oxidation of Ni° active sites in the POM-XANES test.

After the catalytic test, XRD patterns of the spent catalysts were collected, and these are shown in Fig. 5. It can be seen that all samples produce peaks of Ni° (JCPDS 04-0850) after 6 h of reaction. These peaks are weaker in sample NiM, reflecting its resistance to reduction, due to the solid solution formed (resulting in a low concentration of Ni° on the surface of the catalyst), as shown by TPR-XANES (Fig. 1e).

Additionally, Fig. 5 suggests that the addition of MgO to the NiO/ZrO_2 system favored the formation of graphite carbon, since the characteristic peak of this component (26.2°) only appears in the catalysts with higher amounts of MgO (NiM, Ni20MZ and Ni40MZ). The carbon on these catalysts seem not to be prejudicial, since they exhibited higher conversion of methane than NiZ and Ni4MZ catalysts.

4. Conclusions

The results presented here demonstrate that the addition of MgO to NiO/ZrO_2 catalyst synthesized by the one-step chemical polymerization method improved the performance of the catalysts in the POM reaction. Thus, Ni20MZ, Ni40MZ and NiM showed the highest conversion rates and the sample Ni20MZ formed the lowest amount of coke among these catalysts.

XRD analyses showed that Mg^{2+} ions replaced Zr^{4+} in some ZrO_2 unit cells, resulting in contraction of the crystal lattice. In addition, Mg^{2+} entered the NiO unit cells, resulting in the expansion of the crystal lattice of that phase. Synergy between these solid solutions may be involved in the good performance achieved in both the catalytic process and coke removal by the sample with 20 mol% MgO.

The POM-XANES analyses demonstrated that the low POM activity of samples with low and without NiO–MgO solid solution can be explained by the oxidation of Ni° active centers.

Acknowledgements

The authors thank the Brazilian National Council for Scientific Development (CNPq) for the fellowship, the São Paulo Research Foundation (FAPESP), and the Brazilian Synchrotron Light Laboratory (LNLS) in Campinas, Brazil, for the XANES analysis.

References

[1] Rhodes MD, Bell AT. The effects of zirconia morphology on methanol synthesis from CO and H_2 over Cu/ZrO_2 catalysts: Part I. Steady-state studies. J Catal 2005;233:198–209.
[2] Chanchlani KG, Hudgins RR, Silveston PL. Methanol synthesis from H_2, CO, and CO_2 over Cu/ZnO catalysts. J Catal 1992;136:59–75.
[3] Klier K, Chatikavanij V, Herman RG, Simmons GW. Catalytic synthesis of methanol from CO/H_2: IV. The effects of carbon dioxide. J Catal 1982;74:343–60.
[4] Pompeo F, Nichio N, Ferretti O, Resasco D. Study of Ni catalysts on different supports to obtain synthesis gas. Int J Hydrogen Energy 2005;30:1399–405.
[5] Ruckenstein E, Hang-Hu E. Methane partial oxidation over NiO/MgO solid solution catalyst. Appl Catal A 1999;183:85–92.
[6] Choudhary VR, Mamman AS. Oxidative conversion of methane to syngas over NiO/MgO solid solution supported on low surface area catalyst carrier. Fuel Process Technol 1999;60:203–11.
[7] Zhu J, Ommen JGV, Lefferts L. Reaction scheme of partial oxidation of methane to synthesis gas over yttrium-stabilized zirconia. J Catal 2004;225:388–97.
[8] York APE, Xiao T, Green MLH. Brief overview of the partial oxidation of methane to synthesis gas. Top Catal 2003;22:345–58.
[9] Choudhary VR, Mamman AS. Energy efficient conversion of methane to syngas over NiO–MgO solid solution. Appl Energy 2000;66:161–75.
[10] Song YQ, He DH, Xu BQ. Effects of preparation methods of ZrO_2 support on catalytic performances of Ni/ZrO_2 catalysts in methane partial oxidation to syngas. Appl Catal A 2008;337:19–28.
[11] Eriksson S, Rojas S, Boutonnet M, Fierro J. Effect of Ce-doping on Rh/ZrO_2 catalysts for partial oxidation of methane. Appl Catal A 2007;326:8–16.
[12] Enger BC, Lødeng R, Holmen A. Modified cobalt catalysts in the partial oxidation of methane at moderate temperatures. J Catal 2009;262:188–98.
[13] Choque V, Ramírez P, Molyneux D, Homs N. Ruthenium supported on new TiO_2–ZrO_2 systems as catalysts for the partial oxidation of methane. Catal Today 2010;149:248–53.

[14] Yue-Qin S, De-Hua H, Bo-Qing X. Effects of preparation methods of ZrO_2 support on catalytic performances of Ni/ZrO_2 catalysts in methane partial oxidation to syngas. Appl Catal A 2008;337:19–28.
[15] Pengpanich S, Meeyoo V, Rirksomboon T. Methane partial oxidation over Ni/CeO_2–ZrO_2 mixed oxide solid solution catalysts. Catal Today 2004;93–95:95–105.
[16] Kang JS, Kim DH, Lee SD, Hong SI, Moon DJ. Nickel-based tri-reforming catalyst for the production of synthesis gas. Appl Catal A 2007;332:153–8.
[17] Choque V, Homs N, Cicha-Szot R, Ramírez P. Study of ruthenium supported on Ta_2O_5–ZrO_2 and Nb_2O_5–ZrO_2 as catalysts for the partial oxidation of methane. Catal Today 2009;142:308–13.
[18] Marcos PJ, Gouvêa D. Effect of MgO segregation and solubilization on the morphology of ZrO_2 powders during synthesis by the Pechini's method. Cerâmica 2004;50:38–42.
[19] Dong W, Roh H, Jun K, Park S, Oh Y. Methane reforming over Ni/Ce–ZrO_2 catalysts: effect of nickel content. Appl Catal A 2002;226:63–72.
[20] Asencios YJO, Bellido JDA, Assaf EM. Synthesis of NiO–MgO–ZrO_2 catalysts and their performance in reforming of model biogas. Appl Catal A 2011;397:138–44.
[21] Meneses CT, Flores WH, Sotero AP, Tamura E, Garcia F, Sasaki JM. In situ system for X-ray absorption spectroscopy to investigate nanoparticles crystallization. J Synchrotron Rad 2006;13:468–70.
[22] Shannon RD. Revised effective ionic radii and systematic studies of interatomic distances in halides and chalcogenides. Acta Cryst 1976;A32:751–67.
[23] Kroger FA, Vink HJ. Solid State Physic. In: Seitz F, Turnbull D, editors, vol. 3. New York: Academic Press; 1956.
[24] Choudhary VR, Mamman AS. Energy efficient conversion of methane to syngas over NiO–MgO solid solution. Appl Energy 2000;66:161–75.
[25] Hang-Hu Y, Ruckenstein E. The characterization of a highly effective NiO/MgO solid solution catalyst in the CO_2 reforming of CH_4. Catal Lett 1997;43:71–7.
[26] Wen W, Calderon JE, Brito JL, Marinkovic N, Hanson JC, Rodriguez JA. In situ time-resolved characterization of Ni−MoO2 catalysts for the water−gas shift reaction. J Phys Chem C 2008:112–2121.
[27] Profeti LPR, Dias JAC, Assaf JM, Assaf EM. Hydrogen production by steam reforming of ethanol over Ni-based catalysts promoted with noble metals. J Power Sources 2009;190:525–33.
[28] Damynova S, Pawelec B, Arishtirova K, Martinez-Huerta MV, Fierro JLG. Study of the surface and redox properties of ceria–zirconia oxides. Appl Catal A 2008;337:86–96.
[29] Pavizotto NV, Rocha KO, Damyanova S, Passos FB, Zanchet D, Marques CMP, et al. Alumina-supported Ni catalysts modified with silver for the steam reforming of methane: effect of Ag on the control of coke formation. Appl Catal A 2007;330:12–22.
[30] Srinivas D, Satyanarayana CV, Potdar HS, Ratnasamy P. Structural studies on NiO–CeO_2–ZrO_2 catalysts for steam reforming of ethanol (2003). Appl Catal A 2003;246:323–34.
[31] Hu Y, Ruckenstein E. Transient kinetic studies of partial oxidation of CH_4. J Catal 1996;158:260–6.
[32] Bitter J, Seshan K, Lercher J. The state of zirconia supported platinum catalysts for CO_2/CH_4 reforming. J Catal 1997;171:279–86.
[33] Bitter J, Seshan K, Lercher J. Mono and bifunctional pathways of CO_2/CH_4 reforming over Pt and Rh based catalysts. J Catal 1998;176:93–101.
[34] Dow W, Huang T. Yttria-stabilized zirconia supported copper oxide catalyst – I. Effect of oxygen vacancy of support on copper oxide reduction. J Catal 1996;160:155–70.
[35] Xiancai L, Shuigen L, Yifeng Y, Min W, Fei H. Studies on coke formation and coke species of nickel-based catalysts in CO_2 reforming of CH_4. Catal Lett 2007;118:59–63.